International Journal of Solids and Structures 46 (2009) 2201–2215

Contents lists available at ScienceDirect

International Journal of Solids and Structures

journal homepage: www.elsevier.com/locate/ijsolstr

The influence of adhesive constitutive parameters in cohesive zone finite element models of adhesively bonded joints

Peter A. Gustafson, Anthony M. Waas *

Department of Aerospace Engineering, University of Michigan, Ann Arbor, MI 48109, USA

ARTICLE INFO

Article history:
Received 29 February 2008
Received in revised form 19 July 2008
Available online 6 December 2008

Keywords:
Single lap joint
Double cantilever beam
End notch flexure
Adhesive bond
Parameter interaction
Composite
Computer experiments
Fracture
Kriging analysis
Latin hypercube sampling
Toughness
Strength
Sensitivity

ABSTRACT

The influence of adhesive parameters on the outcome of cohesive zone finite element simulations is reported. The simulations are of adhesively bonded joint configurations that are used to characterize joint performance (including the double cantilever beam, the end notch flexure, and the single lap joint). The coupon level experiments are often used individually to determine a single parameter in an adhesive constitutive model (such as a cohesive strength or toughness). In this study, the influence of strength, toughness, and other parameters are considered simultaneously in examining their effect on the finite element (FE) output for each test. In specifying input parameters, the assumed shape of the cohesive traction law is also considered. It is shown that the double cantilever beam model output is dependent primarily on one parameter, whereas the end notch flexure and single lap joint models are dependent on multiple adhesive parameters. By extension, these dependencies require consideration when mapping the results of physical experiments into a set of adhesive model inputs. It is also shown that the shape of the traction law appears insignificant to the outcome of the models. Sensitivities to input parameters are illuminated through kriging analysis of the finite element results; the parameter values are chosen via Latin hypercube sampling. Surrogate models are created and are used to quantify the sensitivities. A mapping technique is described for evaluating the output of physical tests.

1. Introduction

The use of advanced composite materials has increased significantly over the last decade and will be a dominant material for aircraft and spacecraft for the foreseeable future. Composite materials have been used extensively in high performance and military applications, where cost is secondary to performance. However, advances in manufacturing techniques, increased production volumes, environmental concerns, and accumulated field experience have begun to push the technology into the reach of a larger customer base. This base includes commercial aircraft, automotive components, energy generating structures, prosthetic devices, and consumer products.

Technological improvements in composite materials have been accompanied by an improvement in structural adhesives. As a result, the use of bonded joints has begun to enhance or replace the use of traditional mechanical fasteners in composite and metallic structures. In these structures, adhesively bonded joints are now widely used due to improved load distribution, increased service life, reduced machining cost, and/or reduced complexity (Adams et al., 1997). Confidence in such joints has grown with accumulated usage as evidenced by the use of bonded joints in the recent joint strike fighter and the long range strike aircraft programs (Zhang et al., 2006; Bednarcyk et al., 2006). Additionally, the use of adhesively bonded composite joints has expanded into the automotive industry (Pohlit, 2007). Due to their increased use, predictive models of joint performance are needed for better design of joints.

1.1. Literature review: FE methods for joints

Despite decades of development, the design and modeling of bonded joints is an active area of research. Continuum finite element (FE) models of joints began as early as 1971 (Wooley and Carver (1971) and Adams and Peppiatt (1974) are early references).

Abbreviations: ASTM, ASTM International; CC, compliance calibration; CCZM, continuous cohesive zone method; CPE4I, bilinear incompatible mode plain strain elements; DACE, design and analysis of computer experiments; DCB, double cantilever beam; DCZM, discrete cohesive zone method; ENF, end notch flexure; FE, finite element; LEFM, linear elastic fracture mechanics; LHS, Latin hypercube sampling; SLJ, single lap joint; TTL, trapezoidal traction law.

* Corresponding author.
E-mail address: dcw@umich.edu (A.M. Waas).

0020-7683/$ - see front matter © 2008 Elsevier Ltd. All rights reserved.
doi:10.1016/j.ijsolstr.2008.11.016

Nomenclature

A_1	slope of the DCB $a/h - C^{1/3}$ curve	G_{IIc}	mode II critical energy release rate (J/m^2)
$A^{IP}(j)$	surface area associated with a node (m^2)	h	adherend thickness (m)
a_0	crack length (m)	k	initial stiffness (N/m)
α_{pl}	trapezoidal shape factor	l	ENF half span (m)
$\beta_{k,l}$	regression coefficient	μ	friction coefficient
b	specimen width (m)	n	mode mixity exponent
$C(a_0)$	best fit compliance curve (m/N)	P	applied mechanical load (N)
δ	relative nodal displacement (m)	$\overline{P}_{max}$	maximum mechanical load per unit depth (N/m)
D	plate stiffness (Nm)	σ_c	cohesive strength (Pa)
E	modulus (Pa)	σ_{Ic}	cohesive strength in mode I (Pa)
G_c	critical energy release rate (J/m^2)	τ_{IIc}	cohesive strength in mode II (Pa)
G_I	mode I energy release rate (J/m^2)	$\sigma(\delta)$	traction law (Pa)
G_{Ic}	mode I critical energy release rate (J/m^2)	t	adhesive thickness (m)
G_{II}	mode II energy release rate (J/m^2)		

Recent efforts that address strength and durability of joints incorporate elements of fracture mechanics and include the following well known techniques: virtual crack closure technique (Rybicki and Kanninen, 1977; Gillespie et al., 1986; Wang et al., 1994; Glaessgen et al., 1998; Krueger, 2004; Xie et al., 2004, 2005a; Xie and Biggers Jr., 2006). Continuous cohesive zone method (Kafkalidis and Thouless, 2002; Xie et al., 2005b; Li et al., 2005, 2006; Valoroso and Champaney, 2006), discrete cohesive zone method (Hillerborg et al., 1976; Song and Waas, 1994, 1995; Borg et al., 2001, 2002; Xie and Waas, 2006; Xie et al., 2006; Gustafson and Waas, 2007). Though they are perhaps less well known, other adhesive region models have been developed including: Munoz et al. (2006), Goncalves et al. (2002), Goyal et al. (2003), Davies et al. (2006) and Remmers et al. (2003). These references do not constitute an exhaustive list.

Cohesive zone models based on traction laws are well suited to analyzing decohesion in composite structures. In those structures, the length scale associated with the process zone is likely to be larger than any characteristic length of the material (Pietruszczak and Mroz, 1981; Ungsuwarungsri and Knauss, 1987; Tvergaard and Hutchinson, 1992; Schellekens and de Borst, 1993; Xu and Needleman, 1994; Camacho and Ortiz, 1996; Davidson et al., 2000). Cohesive zone models have begun to be incorporated into commercial software including Abaqus® (Simulia, 2007; Camanho and Dávila, 2002) and Genoa® (Alpha STAR, 2008) as well as freely available research codes like Tahoe® (Sandia National Laboratory, 2003).

The discrete cohesive zone method (DCZM) is seen as a promising alternative to the continuous cohesive zone method (CCZM). Continuous cohesive zone elements have been found to be mesh sensitive (in some circumstances), to suffer from convergence difficulty during the softening portion of the cohesive law, and to have sensitivity to aspect ratio (Albouyso et al., 1999; de Borst, 2001, 2003; Zhou and Molinari, 2004). A thorough description of the strengths and weaknesses of the cohesive zone methodologies is provided by Xie et al. (2006). In contrast, the DCZM methodology treats the process zone as a point-wise spring foundation that is discretized to node pairs of adjoining surfaces. The method is scalable to the node spacing and is claimed to be free of mesh dependency (Hillerborg et al., 1976; Pietruszczak and Mroz, 1981; Xie and Waas, 2006). The stiffness matrix is sparse and is therefore computationally efficient. Though it does not avoid instability due to strain softening, careful application of damping stabilization can improve convergence. As a result, a DCZM element is used in this work. The element, shown schematically in Fig. 1 and described in Section 2.1, is implemented as an Abaqus® user element subroutine.

1.2. Traction law considerations

Cohesive zone models require a constitutive law for the adhesive layer; considerable research has focused on experimentally determining the correct law (Olsson and Stigh, 1989; Sørensen, 2002; Alfredsson, 2003; Andersson and Stigh, 2004; Andersson and Biel, 2006; Sørensen and Kirkegaard, 2006; Leffler et al., 2007). Although a precise description of the traction law is important from a fundamental perspective, it may not always be practical or necessary for predictive modeling. In practice, it has been common to assume a parametrized shape for the numerical implementation. In the DCZM element, a traction-separation law is assumed to define the constitutive response of the adhesive layer. The parameters that define the traction law are a critical energy release rate (G_c) and a cohesive strength (σ_c) in each fracture mode. A shape assumption (in this paper, a trapezoid parametrized by α_{pl}) completes the law. Of these defining parameters, G_c and σ_c are often considered to be the most important parameters for the model output (Bazant, 1996; Sørensen and Kirkegaard, 2006).

It is necessary to fully comprehend how model and data reduction assumptions govern fracture prediction in a FE model. Although the determination of G_c and σ_c (or the entire traction law) is necessary for modeling the decohesive behavior of any adhesive or laminated system, it is also necessary to consider the assumptions that are made in computing these values from experimental results. All data reduction techniques make assumptions about the experiments, however, those assumptions may not be correct. For example, it is often assumed that the fracture toughness in mode II (G_{IIc}) can be determined by an end notch flexure (ENF) test independently of other tests. If the assumptions do not hold (in reality or in the context of FE models), traditional methods of mapping the experimental result to a numerical implementation may provide a poor set of parameters for subsequent use in predictive FE modeling.

Some experiments that are commonly used to determine adhesive parameters are the double cantilever beam (DCB) test, the ENF[1] test, and the single lap joint (SLJ) test. In common practice each has been used to determine a specific constitutive parameter (DCB – G_{Ic}, ENF – G_{IIc}, and SLJ – τ_{IIc}). For each experiment, methods have been established for computing the corresponding constitutive parameter based on the measured load and displacement (or

[1] The standard for the ENF test is still evolving (Davidson and Zhao, 2006).

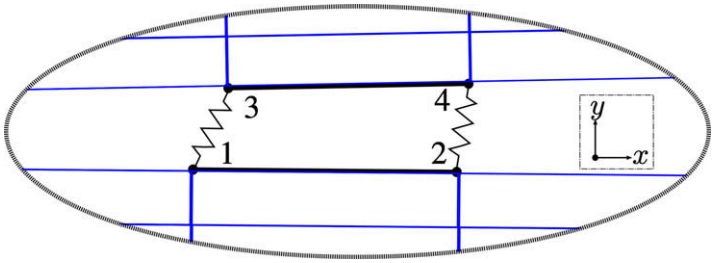

Fig. 1. Four-node 2D DCZM element with surrounding elements. Adhesion is enforced with non-linear 1D sub-elements between node pairs.

other factors). However, there are several uncertainties in each experiment and the computation is not always straightforward.

A critical uncertainty in the experiments is the constitutive response of the adhesive. The shape of the constitutive relation cannot be easily determined and is often assumed or simplified. It has been shown that the shape of the traction law is not important in some cases (Valoroso and Champaney, 2006; Xie and Waas, 2006) and is important in others (Rots, 1986; Chandra et al., 2002; de Borst, 2003; Freed and Banks-Sills, 2008). Fracture modes are often assumed to be decoupled until failure, however, there is little physical justification for this assumption (Högberg et al., 2007). The constitutive uncertainty includes all the parameters that define the shape (i.e. G_c, σ_c, α_{pl}). It is these parameters that are sought in the individual coupon level experiments. Uncertainty also exists in the specimen geometric features, such as the time history of the crack length. Stochastic uncertainty is present in all aspects of the test. In a composite specimen, for example, the adherends consist of fibers and matrix that have undergone a manufacturing cycle. During this cycle, process defects can impact the effective constitution of the adherends. In certain circumstances, these uncertainties can effect the outcome of data reduction of experiments. Consequently, the computed traction law can also be effected.

1.3. Organization and objective

The objective of this paper is to examine the influence of adhesive parameters (such as G_c, σ_c, and α_{pl} in modes I and II) on models of commonly used tests (DCB, ENF, and SLJ) to determine these parameters. For example, it is sought to characterize (in a suitable and quantifiable manner) the effects of G_{IIc}, σ_{Ic}, and τ_{IIc} on the determination of G_{Ic} in a DCB test. Model sensitivity to the adhesive parameters is quantified. The effectiveness of physical experiments are discussed by inference (the discussion is limited to hypothetical data, however, the data are representative of actual experiments). Based on the sensitivities, a method is described by which appropriate parameters can be obtained from a complete set of experimental data. The method combines traditional data-reduction techniques with kriging analysis and the use of a response surface for inverse modeling. Inverse modeling is required to resolve multi-adhesive-parameter dependency in numerical models of the physical experiments.

The paper is organized as follows: Section 2.1 provides a brief introduction to the DCZM element used in the FE models. Section 2.2 reviews standard tests (DCB, ENF, and SLJ) that are used to extract adhesive model parameters. Section 2.3 provides background on kriging analysis and the DACE software (Lophaven, 2002), used for creating a surrogate model. Section 3 reports the model sensitivities to the adhesive parameters. Section 4 examines the implications of the numerical results on the interpretation and data reduction of physical experiments. Final conclusions are presented in Section 5.

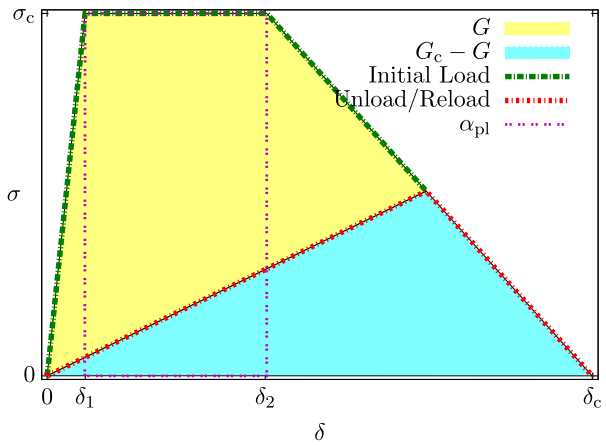

Fig. 2. The trapezoidal traction law.

2. Background

2.1. The DCZM element

The DCZM element is illustrated (in 2D form) in Fig. 1. The element, implemented in Abaqus® as a user element subroutine, consists of non-linear, zero thickness, 1D, spring-like sub-elements between node pairs. Four such sub-elements are used in the 2D version of the element; two are for shear and two are for peel. The 3D version of the element has 12 sub-elements. The relative displacement of the node pairs, transformed into a peel-shear coordinate frame, are used to compute the element force and stiffness from the traction law ($\sigma(\delta)$). For computing stress, the contact area is evenly divided among the nodes pairs of the element. In addition, optional viscous damping is implemented between node pairs to improve convergence (viscosity is used to stabilize the SLJ analysis).[2]

2.1.1. The trapezoidal traction law

A parametrized trapezoidal traction law (TTL) (schematically shown in Fig. 2) was used for modeling decohesion in three standard adhesive tests. The TTL is a widely used traction law (Hillerborg et al., 1976; Ungsuwarungsri and Knauss, 1987; Tvergaard and Hutchinson, 1992; Alfano and Crisfield, 2001; Nguyen et al., 2001; Sørensen, 2002; Xie and Waas, 2006; Xie et al., 2006; Sun, 2007; Gustafson and Waas, 2007, 2008). Implementation is convenient due to the simplicity of formulating the three linear regions of the law. In this paper, the three regions are referred to as: the initial linear response region, the optional "plastic" region, and the strain softening region.

[2] A detailed description of the DCZM implementation is provided in Gustafson and Waas (2007).

Each fracture mode (I, II, and III) requires four parameters to implement the TTL. In two dimensional problems, the required parameters are the critical energy release rates (G_{Ic}, G_{IIc}), the critical strengths (σ_{Ic}, τ_{IIc}), the shape factors ($\alpha_{pl}^{I}, \alpha_{pl}^{II}$) that define the plasticity, and the initial stiffnesses (k_I, k_{II}). In the TTL, the shape factor is the ratio of the rectangular area in the plasticity region to the total area enclosed by the traction law (G_c). Shown in Fig. 2, α_{pl} is bound by zero (restoring a triangular law) and one.

More explicitly, the assumed traction law is:

$$\sigma(\delta) = \begin{cases} k\delta, & \delta < \delta_1, \\ \sigma_c, & \delta_1 \leqslant \delta \leqslant \delta_2, \\ \sigma_c\left(1 - \frac{\delta-\delta_2}{\delta_c-\delta_2}\right), & \delta_2 \leqslant \delta \leqslant \delta_c, \\ 0, & \delta > \delta_c, \end{cases} \tag{1}$$

where the critical relative displacements are given by:

$$\begin{aligned} \delta_1 &= \frac{\sigma_c}{k}, \\ \delta_2 &= \frac{\sigma_c}{k} + \alpha_{pl}\frac{G_c}{\sigma_c}, \\ \delta_c &= (2-\alpha_{pl})\frac{G_c}{\sigma_c}. \end{aligned} \tag{2}$$

Typically, the initial stiffness is large and the strain energy density prior to the initiation of plasticity is small compared to the fracture toughness. Throughout this paper, therefore, the initial stiffness in the traction law is $k = 5 \times 10^{13}$ N/m for mode I and $k = 3 \times 10^{13}$ N/m for mode II.[3]

2.2. Review of the standard tests

In this section, three common adhesive tests are examined. The objective is to identify a model output that correlates to the conventional use of the test. Data reduction uncertainties are also discussed.

2.2.1. The DCB test

The principal objective of the DCB test is to determine G_{Ic} for a given adhesive or inter-laminar interface. The test is well established and commonly used (Roudolff and Ousset, 2002) and a significant body of the literature exists. ASTM International (ASTM) provides recommended procedures for the experiment and for data reduction (ASTM International, 2001b). Three possible data reduction methods are recommended: modified beam theory, compliance calibration (CC), and modified CC. The CC techniques are used to compensate for the material and geometric uncertainties (such as stiffness and initial crack length) that are present in the beam theory solutions. Using the modified CC method, the mode I linear elastic energy release rate (G_I) is:

$$G_I = \frac{3P^2C(a)^{2/3}}{2A_1bh}, \tag{3}$$

where A_1 and $C(a)$ are compliance calibration terms, a is the crack length, b is the specimen width, and h is the adherend thickness. The critical energy release rate (G_{Ic}) requires a "critical load" (P) for each data reduction option. That load can be the maximum load, the point of deviation from linearity, the point of visual delamination, or the so-called 5% increase in compliance.[4] Regardless of the chosen data reduction technique, the computed G_{Ic} depends on the critical load.

With the intent of understanding the sensitivity of the DCB output to the test parameters, it is recognized that all of the DCB data reduction methods find that G_{Ic} is dependent on the square of the critical load (P^2). As a result, the FE sensitivity study (which uses DCZM element) presented in Section 3.1 is motivated by the form of Eq. (3) and uses square of the maximum predicted line load from a 2D analysis[5] ($\overline{P}^2_{max}$) as the model output. In summary, this study presents the sensitivity of $\overline{P}^2_{max}$ to the model inputs.

2.2.2. The ENF test

ASTM has recently resolved to adopt the end notch flexure test as the standard test for determining G_{IIc}, however, the standard has not yet been ratified and is currently evolving (Davidson and Zhao, 2006). As a result, there are several experimental and analysis techniques that have been considered. Davidson and Zhao (2006) have recently evaluated a large number of data reduction techniques, of which only one will be highlighted here.

As in the DCB data reduction techniques, CC can be used to overcome certain geometric and adherend constitutive uncertainties. A CC method for the ENF test (assuming linear elasticity) is:

$$G_{IIc} = \frac{P^2}{2b}\frac{\partial C(a)}{\partial a}\bigg|_{a_0}. \tag{4}$$

In Eq. (4), $C(a)$ is a best fit compliance curve of the form:

$$C(a) = A + ma^3, \tag{5}$$

where $C(a)$ is established by measuring the compliance of a given specimen over a variety of crack lengths. In Eq. (4), G_{IIc} is proportional to the square of the maximum load during the test. Therefore, the sensitivity analysis in Section 3.2 uses $\overline{P}^2_{max}$ as the output of a 2D cohesive zone FE model. As with the DCB test, the ENF data reduction methods assumes that G_{IIc} completely governs the adhesive crack propagation. This assumption will be re-visited in Section 3.2 where the ENF test is analyzed using the DCZM approach.

2.2.3. The SLJ test

The SLJ test is considered next. ASTM claims that the SLJ test is the most widely used test for comparative studies of bonded products (ASTM International, 2001a). It is used to determine the *comparative apparent* shear strength of a given system. Of the three tests discussed in this paper, the SLJ test has the most complex mechanism of failure and is the least able to provide a direct mapping to the desired constitutive parameter (τ_{IIc}).

Although several analytical solutions exist for the stress distribution in a SLJ test,[6] the stress field cannot be uniquely determined due to the reentrant corners in the joint. In practice, the reported output of a SLJ test is the "apparent shear strength", defined as the failure load divided by the lap area. This value is useful only for comparison purposes and is not useful as a constitutive parameter. When the adhesive system is modeled as a cohesive zone (as in this paper), the reentrant corners of the joint are eliminated and a critical shear stress (τ_{IIc}) can more clearly be defined as a constitutive parameter for an assumed traction law. Unfortunately, this does not overcome the complexity of the SLJ test. An appropriate τ_{IIc} must be carefully extracted from the test results.

[3] The initial stiffness is set by: $k = E/t$, where k is based on an assumed tensile modulus (5 GPa), shear modulus (3 GPa), and adhesive thickness (1 mm).

[4] The 5% compliance analysis method uses the initial slope of the load–displacement curve as a reference and establishes the critical load at the intersection the curve with a ray from the origin. The ray has a slope that is 5% lower than the reference slope.

[5] If a 3D FE model were used in place of a 2D model, anticlastic effects would be captured. Due to the normalization of the model output during the kriging analysis, the effects of anticlastic bending are expected to be negligible to the conclusions of this study (Biel and Stigh, 2008).

[6] Volkersen (1938) provided the first shear-lag analytical solution to the SLJ.

To emphasize this point, ASTM provides several recommended procedures for the SLJ test (ASTM International, 2001c, 2005). In doing so, they warn of the risks associated with improper interpretation of the test result. Basic procedures for interpreting the outcome of the SLJ test are given in ASTM International (2001a).[7]

While recognizing the complexity of the SLJ test, it is apparent that the most quantifiable output from the test is the maximum load. Therefore, the sensitivity analysis presented in Section 3.3 uses $\overline{P}_{max}$ as the output from a 2D cohesive zone FE model. In doing so, it illustrates the relationships between the input variables (including the adhesive constitutive parameters) and the experimental output variable.

2.3. Kriging analysis using the DACE toolkit and in association with FE models

To explore the effect of the inputs and their uncertainties on the FE model results, sensitivity studies have been conducted on the three common adhesive tests using kriging analysis[8] and the design and analysis of computer experiments (DACE) toolkit (Lophaven, 2002). Kriging has origins in geostatistical analysis and is used for interpolation between known values in a field. It is also used for optimization in numerical structural analysis. In a typical kriging analysis for that purpose, the outcomes of a set of models are interpolated to obtain an optimality condition. For example, the stress in a structure may be minimized when kriging is used to interpolate the effect of geometric variables.

In each of the FE models of the adhesive tests, a set of variables is identified which may have significant effect on the model output. First among these variables are the adhesive constitutive parameters since they are the parameters of interest. Particular emphasis is placed on the adhesive constitution since the available analytical solutions for each test assume dependency on only one of the adhesive parameters. Therefore, as tools like cohesive elements become available and these parameters become widely used, it is important to determine if the assumptions of the characterization tests are useful in the context of cohesive zone FE models.

The remaining variables (other than constitutive parameters) are chosen based on their likelihood of having significant effect on the model output and for their value as comparative inputs. Several potential variables are deliberately excluded, though they could be included in future work. One excluded variable is adherend plasticity. The adhesive tests are designed to (and are assumed to) result in linear elastic material behavior in the adherends. That assumption is mimicked in this work. Large amounts of plasticity would certainly have effects that are worthy of investigation. However, those effects may distract from the intended interest in the traction law parameters and are therefore excluded. Further, the mixed mode failure criterion for all three tests is not variable and is assumed to be:

$$\left(\frac{G_{\mathrm{I}}}{G_{\mathrm{Ic}}}\right)^{n}+\left(\frac{G_{\mathrm{II}}}{G_{\mathrm{IIc}}}\right)^{n}=1, \tag{6}$$

where the mode mixity exponent (n) is assumed to be one (Whitcomb, 1984; Mi et al., 1998; Dávila, 2001; Alfano and Crisfield, 2001; Reeder, 1992; Dávila and Camanho, 2003; Goyal and Klug, 2004). Finally, the initial stiffness (k) in the traction law is fixed.

Having selected a set of design variables, a range of reasonable values was assigned to each (the variables and their ranges are listed in Tables 1, 3, and 5). The Latin hypercube sampling (LHS) technique (McKay et al., 1979) (incorporated into DACE) was used to create an array of value sets (called sites) for the experimental variables. In LHS (see Fig. 6), the range of each variable is divided into n non-overlapping intervals. A point is sampled randomly from within each interval and the variables combinations are joined randomly from among the intervals (a uniform distribution is assumed within the intervals and equally likely pairings are assumed for the random assignment). The method ensures that the vector space is well represented and that each variable has as many unique values as there are sites. Using LHS, higher order effects and interactions can be identified with fewer sites than in a classical orthogonal array. The reduction in sites facilitates the inclusion of a larger number of variables, including variables which *may not* have significant effect on the model output.[9]

To quickly incorporate the sites into FE models, the FE meshes were parametrized based on the selected variables. The assignment of parameter values to the FE models was managed by an automated shell script (using the *bash* shell on a Linux platform). The script generated individual job files based on the parameter values (the resulting meshes are summarized in Tables 2, 4, and 6 and representative meshes are shown in Figs. 3–5). Job submission, data reduction, and data set compilation were also managed by a set of *bash* shell scripts. The output from each FE model was $\overline{P}^{2}_{max}$ (DCB and ENF models) or $\overline{P}_{max}$ (SLJ model) at crack initiation (defined as the first cohesive element to achieve the failure criterion in Eq. (6)).

The FE models consisted of bilinear incompatible mode plain strain elements (CPE4I) and DCZM elements; the solver was Abaqus® Standard. The adherend material properties were assumed to be orthotropic in-plane and were scaled (relative to the value of E) to be representative of biaxial cloth ($E_{22}=E$, $E_{33}=E/10$, $G_{12}=E/18$, $\nu_{12}=0.30$). Each test was evaluated using DACE (Lophaven, 2002), a package for design and analysis of computer experiments. Analysis based on the kriging technique (McKay et al., 1979) was used to determine the sensitivity of the model output to the input parameters. Critical sensitivities and interactions were found which require consideration when mapping the experimental results to a set of adhesive constitutive parameters.

Data reduction and analysis of the compiled data sets were completed in Octave© using the DACE package. DACE provides a methodology for creation of a surrogate model. A complete description is provided in Lophaven (2002); a brief summary is provided here. The first step in creating the surrogate is normalization of the input and output variables so that each has a mean of zero and a standard deviation of one. The normalization is followed by a regression that relates the normalized output to the input variables; a second order polynomial regression function is used.[10] The regression function and the coefficients $(\beta_{k,l})$[11] that solve the generalized least squares minimization problem (Lophaven, 2002) are the surrogate model. A predictor script can be used to apply the surrogate model to any desired variable site (within the design space). Using the predictor script, a response surface can be generated that is predictive of would-be cohesive zone FE model results.

[7] In the introduction to this standard, it is claimed that the failure load is usually controlled by the tensile stress of the adhesive and not by the shear stress. The results presented in Section 3.3 are more explicit in reporting the relevance of the adhesive constitutive relationship.

[8] A brief summary of kriging analysis is supplied at the end of this section.

[9] These variables are often excluded from an orthogonal array since the number of required runs increases exponentially with the number of variables. The exclusion, based on the best judgment of the analyst, may or may not be appropriate. Conversely, LHS explicitly determines the importance of the variables while minimizing the impact of additional variables on the number of runs that are required.

[10] DACE provides options for several built-in regression functions.

[11] Lophaven (2002) calls $\beta_{k,l}$ the "generalized least squares estimate". For brevity in this paper, they are called coefficients.

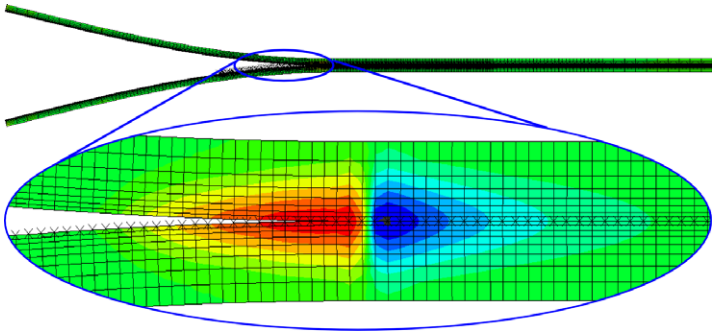

Fig. 3. Typical DCB FE model.

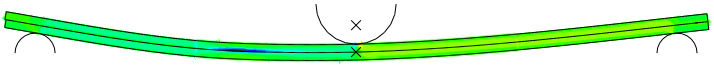

4.1: Global view of the ENF model

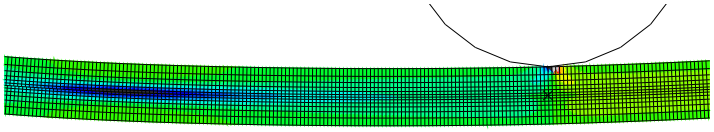

4.2: Local view of the ENF model

Fig. 4. Typical ENF model.

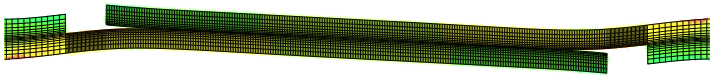

Fig. 5. A typical SLJ finite element model.

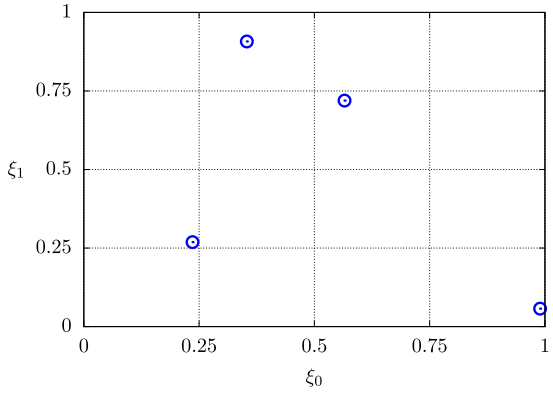

Fig. 6. Example of LHS with two variables and four sites. Each variable takes on four unique values.

The conclusions in this paper are based on the response surface and the properties of the surrogate model itself.[12]

The principal outcome of this study is a quantification of the sensitivity of the output metrics to the input variables. These sensitivities are identified by the regression coefficients ($\beta_{k,l}$) of the surrogate model. Since the regression function is a second order function, each variable has a coefficient for its linear term ("linear coefficient") as well as a coefficient for the product of that variable with each variable ("product coefficient"). The magnitude of the coefficients represents the output sensitivity to the input variables. If an output is highly sensitive to an input, the magnitude of the linear coefficients is approximately one. If an output in insensitive to an input, then the linear coefficients are near zero. Similarly, the magnitudes of the product coefficients are indicative of the relative importance of variable interactions.

The regression coefficients are not independent of the range specified for each variable in the variable array. Care must be taken to choose a range for each variable that is reasonable for a given test. An inappropriate range may overwhelm the other variables and distort the sensitivity conclusions. An appropriate range can best be determined by systematic examination of the $\beta_{k,l}$ coefficients and the surrogate predictions. The predictions must be found reasonable in the context of experimental evidence.

Since the ranges of the variables affect the $\beta_{k,l}$ coefficients, the coefficients should *not* be considered an absolute value. Rather, the relative magnitudes of the coefficients are important. If the magnitude of a coefficient is several times another, the variable has a larger effect on the output. If the magnitude of a coefficient is slightly larger than another coefficient, they have relatively equal importance.

In the following sections, the reported sensitivities to some of the input variables (such as stiffness and crack length) are widely known. These variables are included primarily to determine their relative sensitivity in comparison to the adhesive variables. For

[12] The kriging technique provides prediction of cohesive FE model output. In this paper, trends and close approximations are of interest, therefore, the conclusions are based on the response surface. In traditional uses of kriging such as in design optimization, verification of the optimized site would be required.

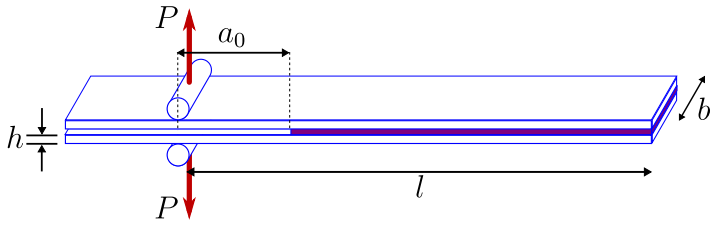

Fig. 7. DCB specimen geometry.

Table 1
Variables in the DCB DACE array.

Variable	Minimum	Maximum
G_{Ic} (J/m^2)	100	1000
G_{IIc} (J/m^2)	100	2000
σ_{Ic} (MPa)	1.5	25
τ_{IIc} (MPa)	2.1	25
α_{pl} (%)	0	50
D (Nm^2)	6.6	21.0
l (mm)	110	150
a_0 (mm)	20	50

these known sensitivities, existing methods (such as compliance calibration) have been developed for compensating for uncertainties. However, the multi-adhesive-parameter dependence of DCB, ENF, and SLJ FE models have not been quantified collectively. The use of a response surface for inverse modeling of adhesive parameters is unique.

Each of the sensitivity studies use a TTL for the DCZM element in the FE model. In doing so, the relative importance of the shape (α_{pl}) of the traction law is included in the sensitivity studies.

3. Sensitivity analysis

3.1. Analysis for the DCB test

A schematic of a DCB specimen, shown in Fig. 7, indicates the geometric variables in the DACE array. In addition to the geometric and material variables, the four primary adhesive parameters (G_{Ic}, G_{IIc}, σ_{Ic}, τ_{IIc}) are included as well as the shape factor (α_{pl}) associated with the TTL. The variables and their ranges are listed in Table 1.[13] A contour plot of a representative peel stress FE result is shown in Fig. 3 and properties of the FE models are provided in Table 2.

Recall that the square of the maximum line load ($\overline{P}^2_{max}$) is related to G_{Ic} and is the output of the DCB model. Since the magnitudes of $\beta_{k,l}$ indicate the sensitivity of $\overline{P}^2_{max}$ to a given variable, $\beta_{k,l}$ is reported.

The linear $\beta_{k,l}$ coefficients for each of the DCB variables are shown in Fig. 8.1. The most important predictor of $\overline{P}^2_{max}$ is G_{Ic}, followed by a_0 and D. The model output, therefore, is most sensitive to G_{Ic}. The product $\beta_{k,l}$ coefficients shown in Fig. 8.2 further confirm these key parameters, since the largest interactions are among these same parameters. This result is not a surprise; the sensitivities to stiffness (D) and crack length (a_0) are widely known and G_{Ic} is *expected* to be proportional to $\overline{P}^2_{max}$ (from linear elastic fracture mechanics (LEFM)). Presumably, D and a_0 are known to a high degree of precision. If they are not, the sensitivity of $\overline{P}_{max}$ to these variables can be accounted by CC methods, though this can be difficult in practice.[14]

[13] The stiffness parameter $\left(D = \frac{Eh^3}{12(1-\nu^2)}\right)$ is included in the DCB and ENF kriging analyses.

[14] The fixed hinge location makes CC of a single specimen difficult.

Table 2
Approximate quantities in the DCB FE model.

Number of elements	5000
Number of user nodes	5300
Number of variables	29,000

An important observation from the $\beta_{k,l}$ coefficients is that G_{Ic} is the only adhesive parameter which has a significant effect on $\overline{P}^2_{max}$. Though this has been assumed in the LEFM based analytical solutions, it has not been previously confirmed in the context of cohesive zone FE modeling techniques. There are no apparent interactions between the adhesive constitutive parameters that would cause significant difficulty in mapping the experimental $\overline{P}^2_{max}$ to a specific G_{Ic} for a cohesive zone FE model. The utility of the DCB test, therefore, is limited primarily by the accuracy of traditional data reduction methods that relate $\overline{P}_{max}$ and other factors to G_{Ic} (see Biel and Stigh (2008) for a discussion of data-reduction accuracy for the DCB test).

Although symmetry exists along the bondline in the DCB specimen, the symmetry was not used in the FE model. The kriging analysis does not recognize the symmetry and is free to find "inappropriate" shear effects in the response. These effects should not exist in the FE model, however, the sensitivity will not be exact zero due to the finite number of samples in the LHS. Not surprisingly, the small sensitivities shown in Fig. 8.1 and 8.2 confirm that the mode II parameters (G_{IIc}, τ_{IIc}) do not effect the outcome of the DCB model. Both the FE model and the regression, therefore, find the symmetry plane to be shear free as required.

To illustrate the relative importance of the variables, Fig. 9 shows the interactions between the two most critical adhesive parameters (G_{Ic}, σ_{Ic}) in the DCB test. In these figures, both of which show the same effect in different forms, G_{Ic} and σ_{Ic} are varied over their specified range while the remaining variables are fixed at their mean values. The value of $\overline{P}^2_{max}$ from the DACE predictor is shown on the z-axis in Fig. 9.1, whereas Fig. 9.2 shows contours of $\overline{P}^2_{max}$ over the same range of inputs. It is apparent that G_{Ic} (the adhesive parameter with the highest $\beta_{k,l}$ coefficient) is far more critical than the second most important adhesive variable. Furthermore, there is little interaction between these two variables (or any other pair of adhesive variables), as evidenced by the near verticality of the contour lines in Fig. 9.2.

The remaining plots in this subsection (Figs. 10–12) illustrate the interactions between the variables G_{Ic}, D, and a_0. For variables with significant interactions, any of a large number of combinations of these parameters will yield the same $\overline{P}^2_{max}$ (in DCB models, significant interactions are present only in the non-adhesive parameters). For example, a large initial crack length (a_0) would decrease $\overline{P}^2_{max}$ relative to a small a_0 (with all other variables fixed) in the same way a lower G_{Ic} would decrease $\overline{P}^2_{max}$ relative to a larger G_{Ic} (with all other variables fixed). The value of $\overline{P}^2_{max}$ is not uniquely defined by one of the two variables. If the model output had significant dependence on multiple adhesive parameters, it would be difficult to map physical test data to a unique G_{Ic}. This difficulty is observed in the upcoming sections covering the ENF and SLJ tests.

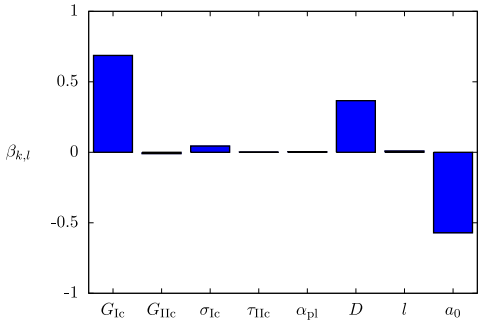

8.1: Linear $\beta_{k,l}$ coefficients for variables in the DCB DACE array

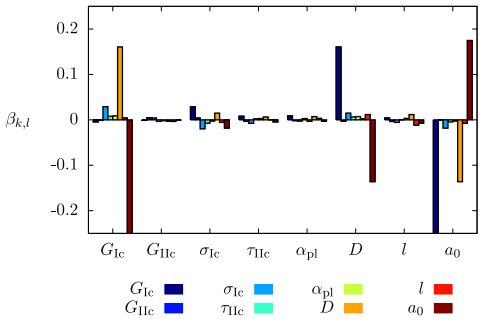

8.2: Product $\beta_{k,l}$ coefficients for variables in the DCB DACE array

Fig. 8. Sensitivity of the DCB model to its inputs.

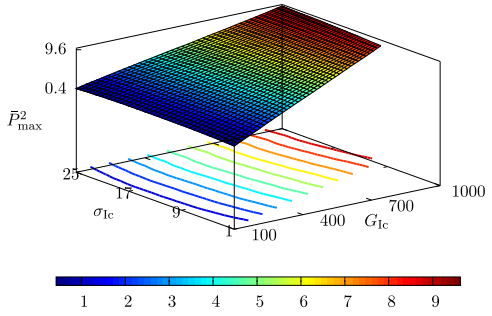

9.1: Surface plot

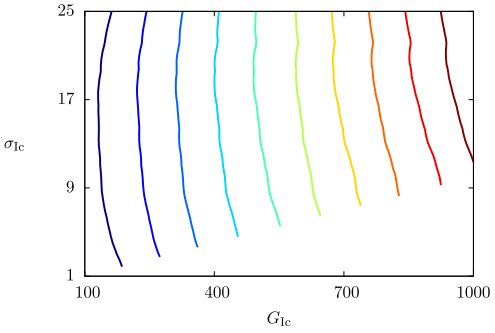

9.2: Contour plot

Fig. 9. Effect of variations of G_{Ic} (J/m^2) and σ_{Ic} (MPa) on $\bar{P}^2_{max}$ (N^2) in the DCB model.

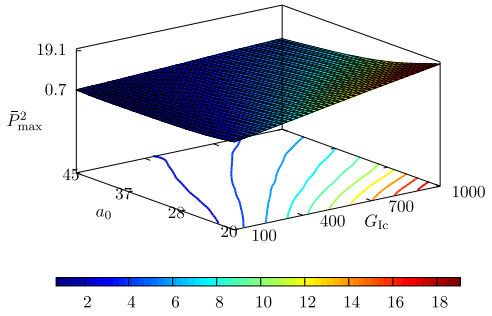

10.1: Surface plot

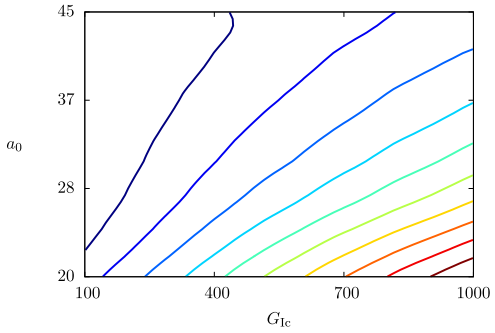

10.2: Contour plot

Fig. 10. Effect of variations of G_{Ic} (J/m^2) and a_0 (mm) on $\bar{P}^2_{max}$ (N^2) in the DCB model.

A final observation from the DCB sensitivity analysis is the relative insensitivity of $\bar{P}^2_{max}$ to the traction law (varied, in this case, by the shape factor α_{pl}). Since the relative magnitude of the linear and product coefficients of $\beta_{k,l}$ are all near zero (see Fig. 8.1 and 8.2), it is concluded that the exact shape of the traction law is not important to the outcome of the prediction. This is to be expected in an experiment that is dominated by the mode I toughness (i.e. the total area under the traction law).

3.2. Analysis for the ENF test

A schematic of a ENF specimen, shown in Fig. 13, indicates the geometric variables in the DACE array. As in the prior section, the four primary adhesive parameters are included in addition to the geometric variables and the shape factor for the TTL. These variables and their ranges are listed in Table 3. Properties of the FE model are given in Table 4 and a typical shear stress contour is shown in Fig. 4.

The principal objective of the ENF test is to determine G_{IIc} for a given adhesive. An accepted method for determining G_{IIc} from an experiment is the CC method (i.e. Eq. (4)); G_{IIc} is expected to be proportional to $\bar{P}^2_{max}$ based on LEFM analysis. Under the assumptions of the CC method, τ_{IIc} has no effect on $\bar{P}^2_{max}$ and therefore is not a factor in the calculation. In this section, that assumption is found to be insufficient in the context of FE cohesive zone modeling.

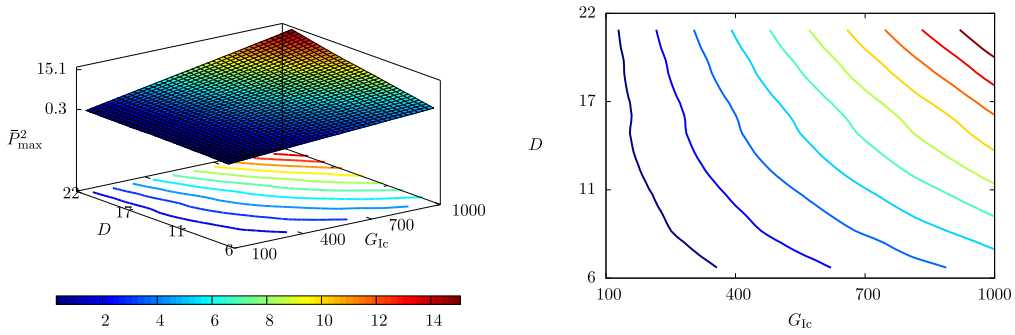

11.1: Surface plot 11.2: Contour plot

Fig. 11. Effect of variations of G_{Ic} (J/m^2) and D (Nm) on $\bar{P}^2_{\max}$ (N^2) in the DCB model.

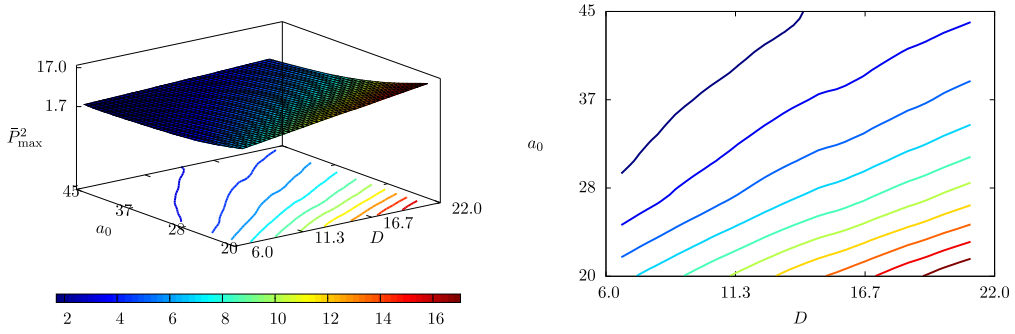

12.1: Surface plot 12.2: Contour plot

Fig. 12. Effect of variations of D (Nm) and a_0 (mm) on $\bar{P}^2_{\max}$ (N^2) in the DCB model.

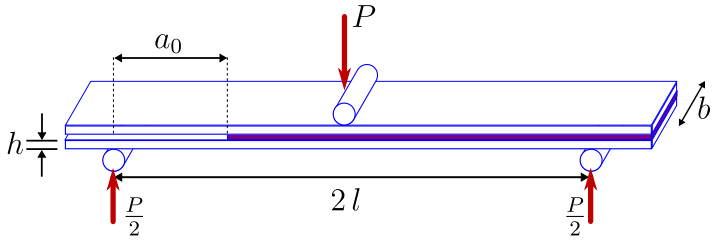

Fig. 13. ENF specimen geometry.

Table 3
Variables in the ENF DACE array.

Variable	Minimum	Maximum
G_{Ic} (J/m^2)	100	1000
G_{IIc} (J/m^2)	100	2000
σ_{Ic} (MPa)	1.5	25
τ_{IIc} (MPa)	2.1	25
α_{pl} (%)	0	50
D (Nm^2)	6.56	21.2
$\frac{a_0}{l}$ (%)	40	90
μ	0	0.50
$2l$ (mm)	96.5	107

Table 4
Approximate quantities in the ENF FE model.

Number of elements	16,000
Number of user nodes	14,000
Number of variables	97,000

The linear $\beta_{k,l}$ coefficients for the DACE variables are shown in Fig. 14.1 and the product $\beta_{k,l}$ coefficients are shown in Fig. 14.2. In the ENF test, G_{IIc} is the most significant of the adhesive parameters; D and $\frac{a_0}{l}$ also have significance. These are *expected* sensitivities based on classical LEFM analysis of the ENF specimen. More importantly, the τ_{IIc} parameter also has an effect on $\bar{P}^2_{\max}$. This conclusion can be visualized in two ways. First, the linear $\beta_{k,l}$ coefficient magnitude for τ_{IIc} (Fig. 14.1) is approximately one fifth that of the $\beta_{k,l}$ coefficient of G_{IIc} (and approximately one third of the coefficients for D and $\frac{a_0}{l}$). Furthermore, the product coefficient for τ_{IIc} and G_{IIc} is non-negligible (as revealed in Fig. 14.2). By generalization to physical tests and based on these observations, the effect of τ_{IIc} on the ENF test *should not be neglected* when mapping experimental results into a set of inputs for cohesive zone FE models. At a minimum, a suitable test for τ_{IIc} (such as the SLJ test) must also be considered when preparing the adhesive constitutive model from the results of the ENF test. This conclusion is more concretely illustrated in

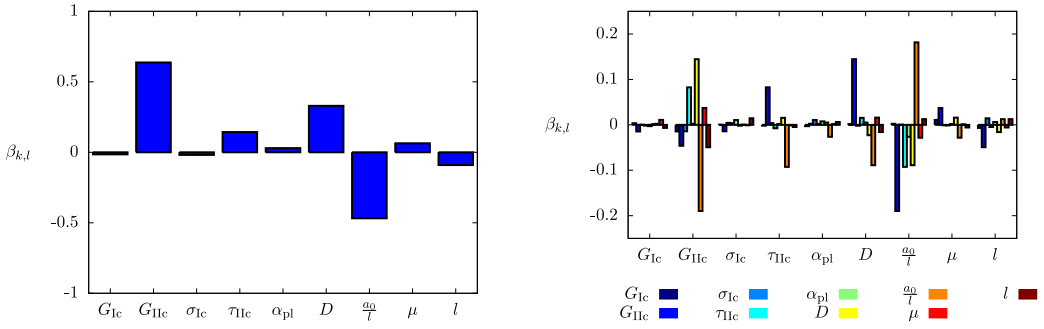

14.1: Linear $\beta_{k,l}$ coefficients for variables in the ENF DACE array

14.2: Product $\beta_{k,l}$ coefficients for variables in the ENF DACE array

Fig. 14. Sensitivity of the ENF model to its inputs.

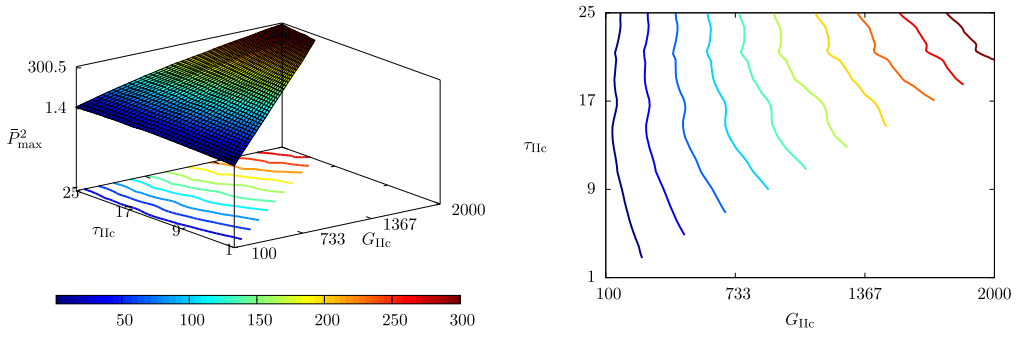

15.1: Surface plot

15.2: Contour plot

Fig. 15. Effect of variations of G_{IIc} (J/m^2) and τ_{IIc} (MPa) on $\bar{P}^2_{max}$ (N^2) in the ENF model.

Fig. 15. In Fig. 15.1, $\bar{P}^2_{max}$ is plotted on the z-axis while the ranges of G_{IIc} and τ_{IIc} are plotted on the x- and y-axes. In contrast to Fig. 9.2, the contour lines in Fig. 15.2 are *not* predominately vertical. A given $\bar{P}^2_{max}$ can be achieved with any suitably chosen pair of (G_{IIc}, τ_{IIc}). In the context of cohesive FE models, the ENF test is *not* ideal for determining G_{IIc}. By extension, the ENF test presents a challenge in mapping physical experimental outcomes back to a set of constitutive parameters for FE models. This mapping should be done in conjunction with an SLJ test and model (or another suitable test) in order to choose an appropriate pairing of constitutive parameters.

An additional observation from the analysis is the insignificance of the traction law. In Fig. 14.1, it is observed that the linear $\beta_{k,l}$ coefficient for the shape parameter (α_{pl}) is relatively small. Further, no critical product $\beta_{k,l}$ coefficients are seen in Fig. 14.2. The traction law is somewhat more important in the ENF test than the DCB test. This is to be expected in a test that has shown some dependency on the stress parameters. However, α_{pl} is still insignificant relative to the other variables. Friction (μ) is slightly more important than α_{pl} to the outcome of the tests, however, it is still insignificant to the overall output.

3.3. Analysis for the SLJ test

Though the SLJ test is viewed as a test for determining the *comparative apparent* τ_{IIc}, it is clear from Section 3.2 that the SLJ test could play a more substantial role in determining the mode II parameters in an adhesive characterization for FE analysis. To understand that role more fully, a sensitivity analysis is completed on models of the SLJ test. A schematic of a SLJ specimen, shown in Fig. 16, indicates the geometric variables in the DACE array. The ranges of those variables are provided in Table 5. A representative shear stress contour is shown in Fig. 5 and properties of the model are given in Table 6.

The linear correlation coefficients $(\beta_{k,l})$ for the SLJ test are shown in Fig. 17.1. There are several parameters that have a significant effect on $\bar{P}_{max}$. As expected, the two largest $\beta_{k,l}$ coefficients are the lap length (l_l) and the critical shear stress (τ_{IIc}). The critical strain energy release rate (G_{IIc}), however, is almost as important as τ_{IIc}. Finally, the mode I critical strain energy release rate (G_{Ic}) is also important due to the eccentric loading of the specimen and mixed-mode field at the crack tip. In contrast to the statements in ASTM International (2001a), it is G_{Ic} (not σ_{Ic}) that has sig-

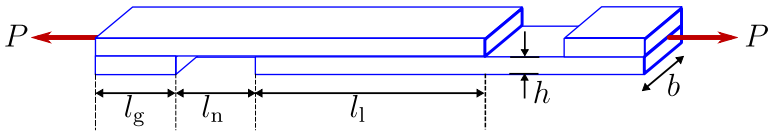

Fig. 16. SLJ specimen geometry.

Table 5
Variables in the SLJ DACE array.

Variable	Minimum	Maximum
G_{Ic} (J/m^2)	100	1000
G_{IIc} (J/m^2)	100	2000
σ_{Ic} (MPa)	1.5	25
τ_{IIc} (MPa)	2.1	25
α_{pl} (%)	0	50
E (GPa)	59.5	80.5
l_l (mm)	10	40
l_g (mm)	2	50
l_n (mm)	2	50
h (mm)	1.06	1.44

Table 6
Approximate quantities in the SLJ FE model.

Number of elements	7400
Number of user nodes	7900
Number of variables	51,000

nificant effect on the failure of the SLJ FE model. This is an important finding of the present work.

The most important interaction in the SLJ model (for establishing a constitutive law) is between G_{IIc} and τ_{IIc}; it is illustrated in Fig. 18. For low G_{IIc}, the maximum load is dependent primarily on τ_{IIc}. In Fig. 18.2, this is seen as contours that are primarily vertical. As G_{IIc} increases, however, the contour lines become more horizontal and the critical energy release rate becomes the dominant parameter for determining $\overline{P}_{max}$. By inference, a physical SLJ test in isolation would be ineffective in determining τ_{IIc} for use in FE models.

A second interaction, between G_{Ic} and G_{IIc}, is illustrated in Fig. 19. For low G_{Ic}, the failure mode is either mode I or mixed-mode such that $\overline{P}_{max}$ is limited by G_{Ic}. For G_{Ic} over a critical value, however, this failure mode no longer dominates and $\overline{P}_{max}$ becomes more dependent on τ_{IIc} and other parameters. A similar effect is seen in Fig. 20.1 and 20.2 relating G_{Ic} to τ_{IIc}.

Fig. 22.2 illustrates the interaction between τ_{IIc} and l_l; the contour lines are almost diagonal. This is expected since $\overline{P}_{max}$ should increase with τ_{IIc} or l_l (for low l_l). A similar interaction is seen between G_{IIc} and l_l as illustrated in Fig. 21.2. By extension to physical experiments in either case, uncertainty in l_l would effect the constitutive parameter extracted from the test.

In summary, three out of the four primary adhesive constitutive parameters are of critical importance in cohesive zone FE models of the SLJ test. Extrapolating to physical test results, it is desirable to simultaneously consider G_{IIc} (based on the ENF test) and G_{Ic} (based on the DCB test) to properly interpret the results of a SLJ test. Only appropriate parameter sets can be used to predict the test outcome in models of all three tests.

4. Discussion

The multi-adhesive-parameter dependence of the adhesive tests (that has been revealed through the sensitivity analysis of the FE models) should be accounted when mapping experimental results into a set of constitutive inputs for FE analysis. This is a sig-

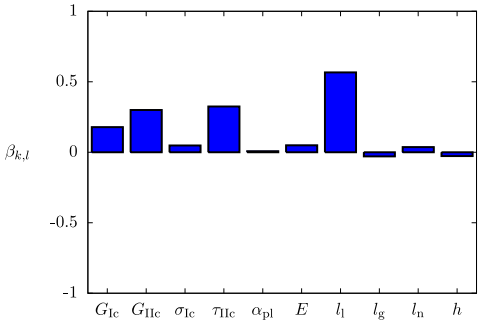

17.1: Linear $\beta_{k,l}$ coefficients for variables in the SLJ DACE array

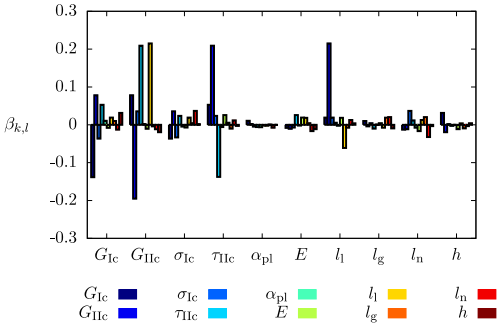

17.2: Product $\beta_{k,l}$ coefficients for variables in the SLJ DACE array

Fig. 17. Sensitivity of the SLJ model to its inputs.

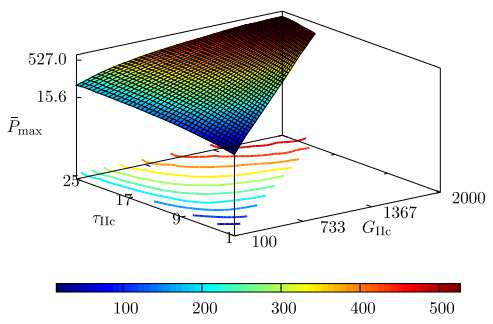

18.1: Surface plot

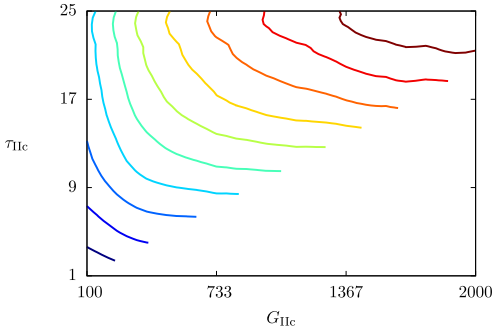

18.2: Contour plot

Fig. 18. Effect of variations of G_{IIc} (J/m^2) and τ_{IIc} (MPa) on $\overline{P}_{max}$ (N) in the SLJ model.

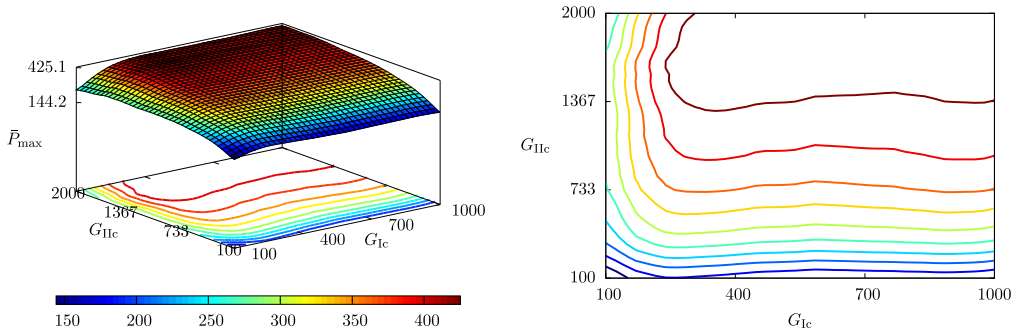

19.1: Surface plot 19.2: Contour plot

Fig. 19. Effect of variations of G_{Ic} (J/m^2) and G_{IIc} (J/m^2) on $\bar{P}_{\max}$ (N) in the SLJ model.

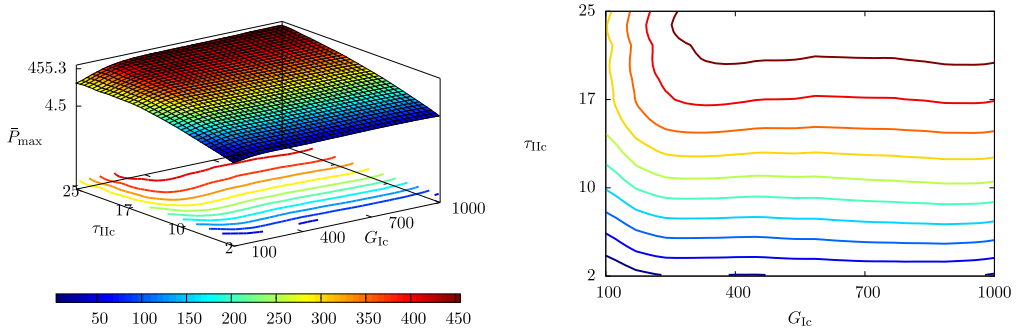

20.1: Surface plot 20.2: Contour plot

Fig. 20. Effect of variations of G_{Ic} (J/m^2) and τ_{IIc} (MPa) on $\bar{P}_{\max}$ (N) in the SLJ model.

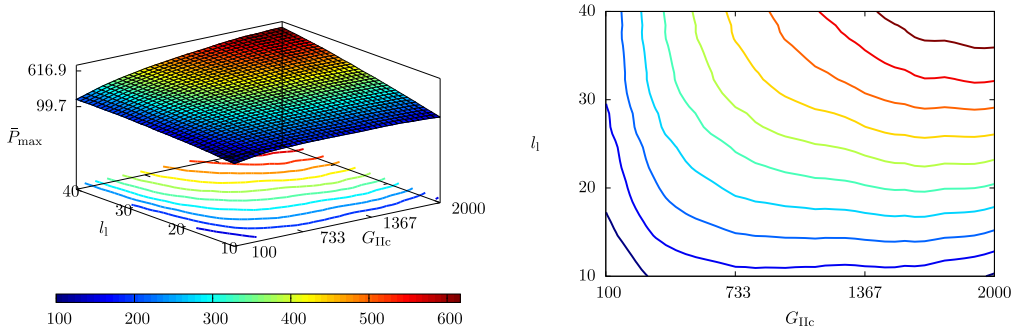

21.1: Surface plot 21.2: Contour plot

Fig. 21. Effect of variations of G_{IIc} (J/m^2) and l_1 (mm) on $\bar{P}_{\max}$ (N) in the SLJ model.

nificant departure from traditional practice where parameters are considered properties that can be uniquely defined by a single test.

A mapping method for data reduction is described next. First, the mode I parameters should be determined using traditional methods (the DCB test for G_{Ic} and an appropriate peel stress test for σ_{Ic}). Subsequently, the ENF test results should be interpreted using traditional CC methods (to determine a distribution of appropriate G_{IIc}). Lastly, the single lap joint test results should be evaluated by inversion in the domain of the response surface. The constitutive parameter values established in the other experiments must be used to determine the appropriate range of τ_{IIc} from the SLJ.

For illustrative purposes, imagine that a series of coupon level DCB and peel stress tests have been completed. As they can reasonably be established in independent tests, a stochastic distribution of G_{Ic} and σ_{Ic} are available from traditional data reduction methods. Further assume that ENF and SLJ tests have been completed to establish distributions of $\bar{P}_{\max}$. According to the mapping procedure, the CC technique can be used with the ENF test results to compute an appropriate distribution of G_{IIc}. Due to the complexity of the SLJ test, τ_{IIc} cannot be directly obtained from the SLJ results. Instead, the surrogate model response surface should be used to obtain a distribution of $(G_{\mathrm{IIc}},\ \tau_{\mathrm{IIc}})$ pairs that would yield the SLJ outcome by a FE model.

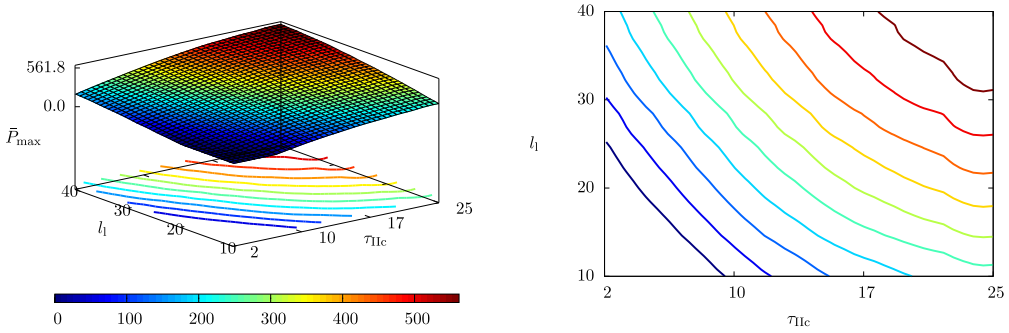

22.1: Surface plot 22.2: Contour plot

Fig. 22. Effect of variations of τ_{IIc} (MPa) and l_1 (mm) on $\bar{P}_{max}$ (N) in the SLJ model.

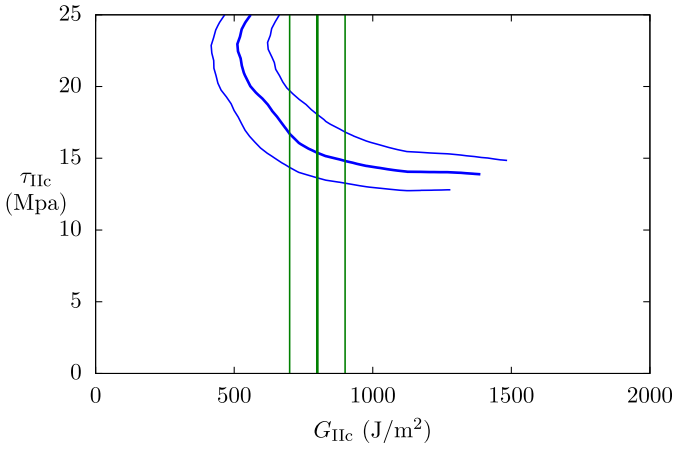

Fig. 23. Hypothetical distribution of appropriate mode II parameters based on parameter mapping. The entire (G_{IIc}, τ_{IIc}) space of the sensitivity analysis is pictured. The appropriate range of parameters is the subspace (intersection) that can be used to obtain correct $\bar{P}_{max}$ distributions for the SLJ and ENF tests.

An example of these last two steps is presented in Fig. 23. The curving blue lines represent sets of (G_{IIc}, τ_{IIc}) pairs that will, by a FE model, produce the correct SLJ $\bar{P}_{max}$ distribution (with all other parameters set at test nominal values). The distribution of appropriate G_{IIc} from the ENF can be overlayed on this plot (the vertical green lines in Fig. 23). The intersection of these distributions are an appropriate set of mode II parameters for (G_{IIc}, τ_{IIc}) for the adherend/adhesive system. Upon finding this intersection of pairs, a complete set of adhesive parameters is established.

5. Conclusion

Sensitivity studies, based on kriging analysis of FE models, have been presented for three experiments (double cantilever beam, end notch flexure, single lap joint) that are commonly used to determine adhesive constitutive parameters. The variables in the studies included two toughness parameters (G_{Ic}, G_{IIc}), two strength parameters $(\sigma_{Ic}, \tau_{IIc})$, and a shape factor for the cohesive traction law (α_{pl}). It is shown that the ENF and SLJ test models are both sensitive to multiple adhesive parameters. By inference, the results of these physical tests should be interpreted together. The DCB model is only sensitive to G_{Ic}, therefore, the DCB test is useful as an independent physical test to determine G_{Ic} for cohesive zone FE models. G_{Ic}, G_{IIc}, and τ_{IIc} each play a non-negligible role in models of the SLJ test. By extension, interpretation of SLJ experimental results is the most difficult. G_{Ic} and G_{IIc} should be considered when mapping the physical SLJ test output to a τ_{IIc} for cohesive zone FE models. Of the three tests that were modeled in the sensitivity studies, no model was significantly effected by σ_{Ic}. By extension, σ_{Ic} can be determined independently in physical tests (given that the experiment for this parameter is considered unlikely to exhibit multi-parameter dependence). Though this conclusion is supported by Mi et al. (1998), independent verification in FE models should be included if a standard test for σ_{Ic} is developed. The results from the present study can be used for mapping a set of experimental results to an appropriate set of FE constitutive parameters for an adhesively bonded joint.

Acknowledgments

This work was supported by the Space Vehicle Technology Institute under Grant NCC3-989 jointly funded by NASA and the Department of Defense. It is managed within the NASA Constellation University Institutes Project, with Claudia Meyer as the project manager and Stanley Smeltzer as the project monitor. P.A. Gustafson also extends gratitude to all contributors to the Octave project, which was used for data reduction.

References

Adams, R.D., Peppiatt, N.A., 1974. Stress analysis of adhesive-bonded lap joints. Journal of Strain Analysis 9 (3), 185–196.

Adams, R., Comyn, J., Wake, W., 1997. Structural Adhesive Joints in Engineering. Chapman & Hall, London.

Albouyso, V., Allix, O., Ladeveze, P., Leveque, D., 1999. Interfacial approach of delamination: possibilities and difficulties. In: Proceedings of the 12th International Conference on Composite Materials, Paris, France.

Alfano, G., Crisfield, M.A., 2001. Finite element interface models for the delamination analysis of laminated composites: mechanical and computational issues. International Journal for Numerical Methods in Engineering 50 (7), 1701–1736. Available from: <http://dx.doi.org/10.1002/nme.93>.

Alfredsson, K., 2003. On the determination of constitutive properties of adhesive layers loaded in shear an inverse solution. International Journal of Fracture 123 (1), 49–62. Available from: <http://dx.doi.org/10.1023/B:FRAC.0000005794.80532.b9>.

Alpha STAR Corp., 2008. GENOA. 5199 East Pacific Coast Highway, Suite 410 Long Beach, California 90804, USA.

Andersson, T., Biel, A., 2006. On the effective constitutive properties of a thin adhesive layer loaded in peel. International Journal of Fracture 141 (1), 227–246. Available from: <http://dx.doi.org/10.1007/s10704-006-0075-6>.

Andersson, T., Stigh, U., 2004. The stress–elongation relation for an adhesive layer loaded in peel using equilibrium of energetic forces. International Journal of Solids and Structures 41 (2), 413–434. Available from: <http://www.sciencedirect.com/science/article/B6VJS-49Y3WT9-5/1/09caba7bd5f1d8e202ee1c6d6012fa74>.

ASTM International, 2001a. ASTM D4896-01 Standard Guide for Use of Adhesive-Bonded Single Lap-Joint Specimen Test Results.

ASTM International, 2001b. ASTM D5528-01 (2007) Standard Test Method for mode I Interlaminar Fracture Toughness of Unidirectional Fiber-Reinforced Polymer Matrix Composites.

ASTM International, 2001c. ASTM D5868-01 Standard Test Method for Lap Shear Adhesion for Fiber Reinforced Plastic (FRP) Bonding.
ASTM International, 2005. ASTM D1002-05 Standard Test Method for Apparent Shear Strength of Single-Lap-Joint Adhesively Bonded Metal Specimens by Tension Loading (Metal-to-Metal).
Bazant, Z.P., 1996. Size effect aspects of measurement of fracture characteristics of quasi-brittle material. Available from: <http://www.sciencedirect.com/science/article/B6TW6-47PFRRJ-5/1/c81273134a39c8f4334da46e179e977c>.
Bednarcyk, B.A., Zhang, J., Collier, C.S., Bansal, Y., Pindera, M.J., 2006. Analysis tools for adhesively bonded composite joints. Part 1: higher-order theory. AIAA Journal 44 (1), 171–180.
Biel, A., Stigh, U., 2008. Effects of constitutive parameters on the accuracy of measured fracture energy using the DCB-specimen. Engineering Fracture Mechanics 75 (10), 2968–2983. Available from: <http://www.sciencedirect.com/science/article/B6V2R-4RJ9X6G-2/1/656381ee91d697f188321f60e7d7bd80>.
Borg, R., Nilsson, L., Simonsson, K., 2001. Simulation of delamination in fiber composites with a discrete cohesive failure model. Composites Science and Technology 61 (5), 667–677. Available from: <http://www.sciencedirect.com/science/article/B6TWT-42TC70X- 4/1/643eab63e1505dc5c927fa172e1c8474>.
Borg, R., Nilsson, L., Simonsson, K., 2002. Modeling of delamination using a discretized cohesive zone and damage formulation. Composites Science and Technology 62 (10–11), 1299–1314. Available from: <http://www.sciencedirect.com/science/article/B6TWT-45X2NNB-1/1/d8533107f75560b8bcc9fdeb7e61a1b2>.
Camacho, G., Ortiz, M., 1996. Computational modelling of impact damage in brittle materials. International Journal of Solids and Structures 33 (20), 2899–2938.
Camanho, P., Dávila, C., 2002. Mixed-mode decohesion finite elements for the simulation of delamination in composite materials. Tech. Rep. TM-2002-211737, NASA.
Chandra, N., Li, H., Shet, C., Ghonem, H., 2002. Some issues in the application of cohesive zone models for metal-ceramic interfaces. International Journal of Solids and Structures 39 (10), 2827–2855. Available from: <http://www.sciencedirect.com/science/article/B6VJS-45CVXXR-4/1/7c332dce346f135f36f5027d7dce8136>.
Davidson, B.D., Zhao, W., 2006. An accurate mixed-mode delamination failure criterion for laminated fibrous composites requiring limited experimental input. Journal of Composite Materials. 0021998306071031. Available from: <http://jcm.sagepub.com/cgi/content/abstract/0021998306071031v1>.
Davidson, B.D., Gharibian, S.J., Yu, L., 2000. Evaluation of energy release rate-based approaches for predicting delamination growth in laminated composites. International Journal of Fracture 105 (4), 343–365. Available from: <http://dx.doi.org/10.1023/A:1007647226760>.
Davies, G., Hitchings, D., Ankersen, J., 2006. Predicting delamination and debonding in modern aerospace composite structures. Composites Science and Technology 66 (6), 846–854. Available from: <http://www.sciencedirect.com/science/article/B6TWT-4FF8WMX-G/2/ed3551aaf5771a3d9bebf34439e8b356>.
Dávila, C.G., 2001. Mixed-mode decohesion elements for analysis of progressive delamination. In: 42nd AIAA/ASME/ASCE/AHS/ASC Structures, Structural Dynamics, and Materials Conference.
Dávila, C., Camanho, P., 2003. Analysis of the effects of residual strains and defects on skin/stiffener debonding using decohesion elements. In: 44th AIAA/ASME/ASCE/AHS/ASC Structures, Structural Dynamics, and Materials Conference.
de Borst, R., 2001. Some recent issues in computational failure mechanics. International Journal for Numerical Methods in Engineering 52 (5), 63–96.
de Borst, R., 2003. Numerical aspects of cohesive-zone models. Engineering Fracture Mechanics 70 (14), 1743–1757. Available from: <http://www.sciencedirect.com/science/article/B6V2R-48FSTX5-2/2/57c9eb760e7fd63edfff18c03f488143>.
Freed, Y., Banks-Sills, L., 2008. A new cohesive zone model for mixed mode interface fracture in bimaterials. Engineering Fracture Mechanics 75 (15), 4583–4593.
Gillespie Jr., J.W., Carlsson, L.A., Pipes, R.B., 1986. Finite element analysis of the end notched flexure specimen for measuring mode ii fracture toughness. Composites Science and Technology 27 (3), 177–197. Available from: <http://www.sciencedirect.com/science/article/B6TWT-481DNGV-4B/2/010cd41c9bf3d161476628b14c43278a>.
Glaessgen, E., Raju, I., Poe Jr., C.C., 1998. Fracture mechanics analysis of stitched stiffener-skin debonding. In: 39th AIAA/ASME/ASCE/AHS/ASC Structures, Structural Dynamics, and Materials Conference. No. 98-2022.
Goncalves, J.P.M., de Moura, M.F.S.F., de Castro, P.M.S.T., 2002. A three-dimensional finite element model for stress analysis of adhesive joints. International Journal of Adhesion and Adhesives 22 (5), 357–365. Available from: <http://www.sciencedirect.com/science/article/B6TW7-46MNK9F-2/2/26413fbaf8b669ecfd067ff9470e36fe>.
Goyal, V.K., Klug, J.C., 2004. Interphasic Formulation for the Prediction of Delamination, 1845–2004.
Goyal, V.K., Johnson, E.R., Cassino, C., 2003. Computational model for progressive failure of adhesively bonded joints. In: 44th AIAA/ASME/ASCE/AHS/ASC Structures, Structural Dynamics, and Materials Conference.
Gustafson, P.A., Waas, A.M., 2007. T650/AFR-PE-4/FM680-1 mode I critical energy release rate at high temperatures: experiments and numerical models. In: Proceedings of the AIAA/ASME/ASCE/AHS/ASC 48th Structures, Structural Dynamics, and Materials Conference, April 23–26, 2007, Honolulu HI, No. 2007-2305, American Institute of Aeronautics and Astronautics.
Gustafson, P.A., Waas, A.M., 2008. Efficient and robust traction laws for the modeling of adhesively bonded joints. In: Proceedings of the AIAA/ASME/ASCE/AHS/ASC 49th Structures, Structural Dynamics, and Materials Conference, April 7–10, 2008, Schaumburg, IL, No. 2008-1847, American Institute of Aeronautics and Astronautics.
Hillerborg, A., Modeer, M., Petersson, P., 1976. Analysis of crack formation and crack growth in concrete by means of fracture mechanics and finite elements. Cement and Concrete Research 6, 773–782.
Högberg, J., Sørensen, B., Stigh, U., 2007. Constitutive behaviour of mixed mode loaded adhesive layer. International Journal of Solids and Structures 44 (25–26), 8335–8354. Available from: <http://www.sciencedirect.com/science/article/B6VJS-4P192N5-6/1/e69566e358f4aa9a45f0c3b86a00440f>.
Kafkalidis, M.S., Thouless, M.D., 2002. The effects of geometry and material properties on the fracture of single lap-shear joints. International Journal of Solids and Structures 39 (17), 4367–4383. Available from: <http://www.sciencedirect.com/science/article/B6VJS-46MD31M-B/2/0a781a592c8a429a39b77273714ad9e1>.
Krueger, R., 2004. Virtual crack closure technique: history, approach, and applications. Applied Mechanics Reviews 57 (2), 109–143. Available from: <http://link.aip.org/link/?AMR/57/109/1>.
Leffler, K., Alfredsson, K., Stigh, U., 2007. Shear behaviour of adhesive layers. International Journal of Solids and Structures 44 (2), 530–545. Available from: <http://www.sciencedirect.com/science/article/B6VJS-4JWDY4B-1/1/cf1ac90c1b19b5c502241fe7f322ffc0>.
Li, S., Thouless, M., Waas, A., Schroeder, J., Zavattieri, P., 2005. Use of a cohesive-zone model to analyze the fracture of a fiber-reinforced polymer–matrix composite. Composites Science and Technology 65 (3–4), 537–549. Available from: <http://www.sciencedirect.com/science/article/B6TWT-4DTKG5G-1/2/294d076eab59de1821bd8b5e2f1e3ebf>.
Li, S., Thouless, M., Waas, A., Schroeder, J., Zavattieri, P., 2006. Competing failure mechanisms in mixed-mode fracture of an adhesively bonded polymer–matrix composite. International Journal of Adhesion and Adhesives 26 (8), 609–616. Available from: <http://www.sciencedirect.com/science/article/B6TW7-4HM82MP-1/2/8d7a9c11e2eab46c8212b19e9ef40cdd>.
Lophaven, S.N., August 2002. DACE: a Matlab Kriging Toolbox. Technical University of Denmark, DK-2800 Kgs, Lyngby, Denmark, version 2.0 Edition. Available from: <http://www2.imm.dtu.dk/~hbn/dace/>.
McKay, M., Beckman, R., Conover, W., 1979. A comparison of three methods for selecting values of input variables in the analysis of output from a computer code. Technovation 21 (2), 239–245.
Mi, Y., Crisfield, M.A., Davies, G.A.O., Hellweg, H.B., 1998. Progressive delamination using interface elements. Journal of Composite Materials 32 (14), 1246–1272. Available from: <http://jcm.sagepub.com/cgi/content/abstract/32/14/1246>.
Munoz, J., Galvanetto, U., Robinson, P., 2006. On the numerical simulation of fatigue driven delamination with interface elements. International Journal of Fatigue 28 (10), 1136–1146. Available from: <http://www.sciencedirect.com/science/article/B6V35-4JHMHXB-1/2/c0a7404dab82160a13b015fa89eb4a48>.
Nguyen, O., Repetto, E., Ortiz, M., Radovitzky, R., 2001. A cohesive model of fatigue crack growth. International Journal of Fracture 110 (4), 351–369. Available from: <http://dx.doi.org/10.1023/A:1010839522926>.
Olsson, P., Stigh, U., 1989. On the determination of the constitutive properties of thin interphase layers G an exact inverse solution. International Journal of Fracture 41 (4), R71–R76. Available from: <http://dx.doi.org/10.1007/BF00018870>.
Pietruszczak, S., Mroz, Z., 1981. Finite element analysis of deformation of strain-softening materials. International Journal for Numerical Methods in Engineering 17 (3), 327–334.
Pohlit, D.J., 2007. Dynamic mixed-mode fracture of bonded composite joints for automotive crashworthiness, Master's Thesis, Virginia Polytechnic Institute and State University.
Reeder, J., 1992. An evaluation of mixed-mode delamination failure criteria. Tech. Rep., NASA.
Remmers, J.J.C., Borst, R.D., Needleman, A., 2003. A cohesive segments method for the simulation of crack growth. Computational Mechanics 31 (1), 69–77. Available from: <http://dx.doi.org/10.1007/s00466-002-0394-z>.
Rots, J., 1986. Strain-softening analysis of concrete fracture specimens. Fracture Toughness and Fracture Energy of Concrete, 150–153.
Roudolff, F., Ousset, Y., 2002. Comparison between two approaches for the simulation of delamination growth in a.d.c.b. specimen. Aerospace Science and Technology 6 (2), 123–130. Available from: <http://www.sciencedirect.com/science/article/B6VK2-45MCM8X-4/2/81862a196fd3fd0dd9e76f6197f3fdcb>.
Rybicki, E.F., Kanninen, M.F., 1977. A finite element calculation of stress intensity factors by a modified crack closure integral. Engineering Fracture Mechanics 9 (4), 931–938. Available from: <http://www.sciencedirect.com/science/article/B6V2R-481FXR6-74/2/e16247ed90259d3b246438c40430c709>.
Sandia National Laboratory, 2003. Tahoe User Guide, third ed., May 2003. Available from: <https://tahoe.ca.sandia.gov/public/doc/tahoe.user.pdf>.
Schellekens, J., de Borst, R., 1993. On the numerical integration of interface elements. International Journal for Numerical Methods in Engineering 36 (43–66), 30–31.
Simulia, I., 2007. Abaqus User Manual v6.7, Electronic Version.
Song, S.J., Waas, A.M., 1994. Mode I failure of laminated polymeric composites. Engineering Fracture Mechanics 49 (1), 17–27.
Song, S.J., Waas, A.M., 1995. Energy-based mechanical model for mixed mode failure of laminated composites. AIAA Journal 33 (4), 739–745.
Sørensen, B.F., 2002. Cohesive law and notch sensitivity of adhesive joints. Acta Materialia 50 (5), 1053–1061. Available from: <http://www.sciencedirect.com/science/article/B6TW8-4567RFW-F/1/bed7c6f573d1dc933e4bb770e9530f49>.

Sørensen, B.F., Kirkegaard, P., 2006. Determination of mixed mode cohesive laws. Engineering Fracture Mechanics 73 (17), 2642–2661. Available from: <http://www.sciencedirect.com/science/article/B6V2R-4K7NHRW-1/1/38f4c53e7d52eb336ce8a32052495751>.

Sun, C., 2007. Fracture of plastically deforming, adhesively bonded structures: experimental and numerical studies, Ph.D. Thesis, University of Michigan, Co-chairs: Anthony M. Waas and Michael D. Thouless.

Tvergaard, V., Hutchinson, J., 1992. The relation between crack growth resistance and fracture process parameters in elastic–plastic solids. Journal of the Mechanics and Physics of Solids 40 (6), 1377–1397.

Ungsuwarungsri, T., Knauss, W., 1987. The role of damage-softened material behavior in the fracture of composites and adhesives. International Journal of Fracture 35 (3), 221–241.

Valoroso, N., Champaney, L., 2006. A damage-mechanics-based approach for modelling decohesion in adhesively bonded assemblies. Engineering Fracture Mechanics 73 (18), 2774–2801. Available from: <http://www.sciencedirect.com/science/article/B6V2R-4KCGJ28-2/2/39c784695ef1a0530c4bb222bb1f3631>.

Volkersen, O., 1938. Die niektraftverteilung in zugbeanspruchten mit konstanten laschenquerschritten. Luftfahrtforschung 15, 41–47.

Wang, J.T., Raju, I.S., Sleight, D.W., 1994. Fracture mechanics analyses of composite skin-stiffener debond configurations with shell elements. No. 94-1389-CP.

Whitcomb, J., 1984. Analysis of instability-related growth of a through-width delamination. Tech. Rep., NASA.

Wooley, G.R., Carver, D.R., 1971. Stress concentration factors for bonded lap joints. Journal of Aircraft 8, 817–820.

Xie, D., Biggers Jr., S.B., 2006. Progressive crack growth analysis using interface element based on the virtual crack closure technique. Finite Elements in Analysis and Design 42 (11), 977–984.

Xie, D., Waas, A.M., 2006. Discrete cohesive zone model for mixed-mode fracture using finite element analysis. Engineering Fracture Mechanics 73 (13), 1783–1796. Available from: <http://www.sciencedirect.com/science/article/B6V2R-4JWMT9S-1/2/cb7f2ffbf807df7034ed78a45863e081>.

Xie, D., Waas, A.M., Shahwan, K.W., Schroeder, J.A., Boeman, R.G., 2004. Computation of energy release rates for kinking cracks based on virtual crack closure technique. Computer Modeling in Engineering and Sciences 6, 515–524.

Xie, D., Salvi, A.G., Waas, A.M., Caliskan, A., 2005a. Discrete cohesive zone model to simulate static fracture in carbon fiber textile composites. In: 46th AIAA/ASME/ASCE/AHS/ASC Structures, Structural Dynamics, and Materials Conference.

Xie, D., Waas, A.M., Shahwan, K.W., Schroeder, J.A., Boeman, R.G., 2005b. Fracture criterion for kinking cracks in a tri-material adhesively bonded joint under mixed mode loading. Engineering Fracture Mechanics 72 (16), 2487–2504. Available from: <http://www.sciencedirect.com/science/article/B6V2R-4G9GNPF-1/2/7d3d2605a8aaac89c387468867ccdc38>.

Xie, D., Salvi, A.G., Sun, C., Waas, A.M., Caliskan, A., 2006. Discrete cohesive zone model to simulate static fracture in 2D triaxially braided carbon fiber composites. Journal of Composite Materials. Available from: <http://jcm.sagepub.com/cgi/content/abstract/0021998306061320v1>.

Xu, X., Needleman, A., 1994. Numerical simulations of fast crack growth in brittle solids. Journal of the Mechanics and Physics of Solids 42 (9), 1397–1407.

Zhang, J., Bednarcyk, B.A., Collier, C., Yarrington, P., Bansal, Y., Pindera, M.J., 2006. Analysis tools for adhesively bonded composite joints. Part 2: unified analytical theory. AIAA Journal 44 (8), 1709–1719.

Zhou, F., Molinari, J., 2004. Dynamic crack propagation with cohesive elements: a methodology to address mesh dependency. International Journal for Numerical Methods in Engineering 59, 1–24.